*The ISME Journal*, 2026, 20(1), wrag021
https://doi.org/10.1093/ismejo/wrag021
Published: 10 February 2026
**Original Article**

# Thermophilic bacteria employ a contractile injection system in hot spring microbial mats

Vasil A. Gaisin[1,‡,*], Corina Hadjicharalambous[1,‡], Izabela Mujakić[2], Cristian Villena-Alemany[2,3], Jiangning Li[1,4], Michal Koblížek[2], Martin Pilhofer[1,*]

[1]Department of Biology, Institute of Molecular Biology & Biophysics, Eidgenössische Technische Hochschule Zürich, Otto-Stern-Weg 5, 8093 Zürich, Switzerland
[2]Laboratory of Anoxygenic Phototrophs, Institute of Microbiology of the Czech Academy of Sciences, Novohradská 237, 37901 Třeboň, Czechia
[3]Current affiliation: Department of Plankton and Microbial Ecology, Leibniz Institute of Freshwater Ecology and Inland Fisheries, Stechlin, Germany
[4]Current affiliation: Biozentrum, University of Basel, 4056 Basel, Switzerland

*Corresponding authors. Martin Pilhofer, Department of Biology, Institute of Molecular Biology & Biophysics, Eidgenössische Technische Hochschule Zürich, Otto-Stern-Weg 5, 8093 Zürich, Switzerland. E-mail: pilhofer@biol.ethz.ch; Vasil A. Gaisin, Department of Biology, Institute of Molecular Biology & Biophysics, Eidgenössische Technische Hochschule Zürich, Otto-Stern-Weg 5, 8093 Zürich, Switzerland. E-mail: vasil.gaisin@mol.biol.ethz.ch
‡Vasil A. Gaisin and Corina Hadjicharalambous contributed equally to this work

## Abstract

Bacterial contractile injection systems (CISs) are multiprotein complexes that facilitate the bacterial response to environmental factors or interactions with other organisms. Multiple novel CISs have been characterised in laboratory bacterial cultures recently; however, studying CISs in the context of the native microbial community remains challenging. Here, we present an approach to characterise a bioinformatically predicted CIS by directly analysing bacterial cells from their natural environment. Using cryo-focused ion beam milling and cryo-electron tomography (cryoET) imaging, guided by 16S rRNA gene amplicon sequencing, we discovered that thermophilic *Chloroflexota* bacteria produce intracellular CIS particles in a natural hot spring microbial mat. We then found a niche-specific production of CIS in the structured microbial community using an approach combining metagenomics, proteomics, and immunogold staining. Bioinformatic analysis and imaging revealed CISs in other extremophilic *Chloroflexota* and *Deinococcota*. This *Chloroflexota*/*Deinococcota* CIS lineage shows phylogenetic and structural similarity to previously described cytoplasmic CIS from *Streptomyces* and probably shares the same cytoplasmic mode of action. Our integrated environmental cryoET approach is suitable for discovering and characterising novel macromolecular complexes in environmental samples.

## Graphical abstract

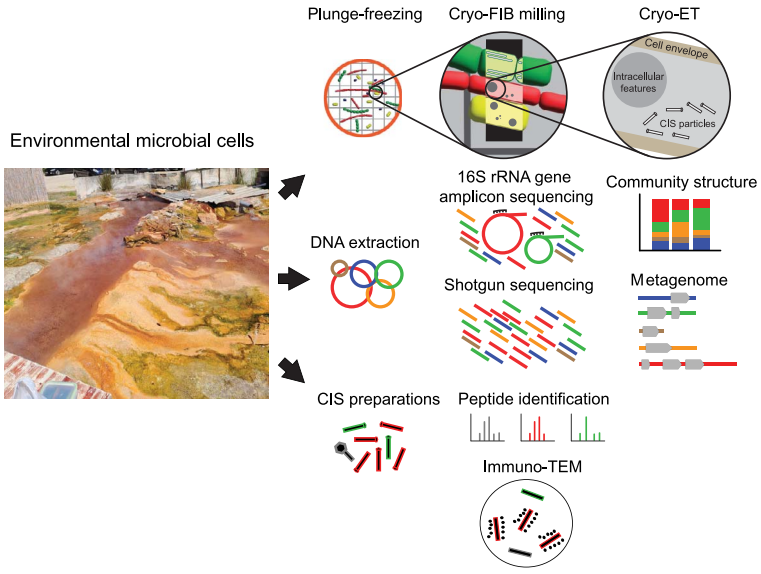


**Received:** 1 September 2025. **Revised:** 19 January 2026. **Accepted:** 6 February 2026
© The Author(s) 2026. Published by Oxford University Press on behalf of the International Society for Microbial Ecology.
This is an Open Access article distributed under the terms of the Creative Commons Attribution License (https://creativecommons.org/licenses/by/4.0/), which permits unrestricted reuse, distribution, and reproduction in any medium, provided the original work is properly cited.

Downloaded from https://academic.oup.com/ismej/article/20/1/wrag021/8471199 by guest on 16 March 2026

***Keywords*** cryo-electron tomography, cryo-focused ion beam milling, *in situ* imaging, immunogold labelling, extremophiles, *Chloroflexota, Roseiflexus castenholzii*

## Introduction

Microorganisms drive many important biogeochemical processes on our planet. Their growth is determined by basic physicochemical conditions, but it also depends on interactions between different microbial species and between individual cells of a single species. These interactions are often facilitated by multiprotein complexes, such as archaeal and bacterial contractile injection systems (CISs) [1]. CISs show homology to contractile phage tails and act as nanoscale syringes injecting cargo molecules, often toxic effectors, into a target cell [2]. The architecture of diverse CISs is conserved and comprises a contractile sheath surrounding an inner tube, as well as a baseplate module. The triggered baseplate initiates CIS firing through sheath contraction and inner-tube expulsion [3]. Assembled CIS particles can have different cellular localisations, which dictate their mode of action. The type-six secretion system (T6SS) is a CIS anchored in the cytoplasmic membrane that injects effector proteins from the cytoplasm into target cells [4, 5]. Extracellular CIS (eCIS) are found free-floating in the cytoplasm before being released to the extracellular space to target other cells [6–8]. The thylakoid-anchored CIS fires while being anchored in the cyanobacterial thylakoid membrane stacks [9]. The cytoplasmic CIS (cCIS) resembles eCIS; however, it is targeted to induce cell death in the CIS-producing cells upon stress, without being released into the environment [10–12].

The thylakoid-anchored CIS, eCIS from *Algoriphagus machipongonensis*, and T6SS subtype 4 from "*Candidatus* Amoebophilus asiaticus" cluster within a single phylogenetic clade and share clade-specific structural proteins, despite having distinct modes of action [6]. Therefore, predictions of CIS mode of action can be unreliable when based only on sequencing data. However, when sequencing data and high-resolution *in situ* imaging of CISs are combined, the CIS mode of action can be identified more confidently. A key technology for imaging CIS in their cellular context in a near-native flash-frozen state is cryo-electron tomography (cryoET) [13]. CryoET has become a powerful tool for *in situ* imaging, resulting in high-resolution and 3D reconstructions (cryo-tomograms) of cellular structure [14]. CryoET, however, is limited to relatively thin samples—up to ∼500 nm of thickness. Hence, cryo-focused ion beam milling (cryoFIB) is often required to thin thicker samples and generate so-called lamellae that can be subsequently imaged by cryoET [14].

Previous studies of CISs have focused on model organisms that can be cultured in the lab. To better understand how bacterial CISs are employed in natural environments, we set out to investigate a novel CIS produced by a natural bacterial population. We chose a *Roseiflexus*-dominated microbial mat as a model system for three main reasons. First, bacteria of the genus *Roseiflexus* possess CIS-like genes in their genomes [15–17]. Second, *Roseiflexus* bacteria have been found in hot springs worldwide [18]. Third, *Roseiflexus* cells form a relatively large and prominent population in microbial mats [19–21]. Hot spring microbial mats have a stable multilayer organisation, which makes them a convenient model system for *in situ* studies of ecophysiological processes and microbial interactions that govern spatially structured microbial communities [19, 22]. However, due to the complexity and size of the mats, we had to tackle significant challenges in making these environmental samples amenable to cryoET imaging and in integrating this technique with approaches from microbial ecology. Here we employed the combination of conventional "omics" techniques with cryoFIB/ET and immuno-TEM, to investigate hot spring mats at the levels of microbial communities, cells, and macromolecular complexes, resulting in the discovery of previously uncharacterised CISs.

## Materials and methods

### Bacterial strains and growth medium

*Roseiflexus castenholzii* DSM 13941$^T$, *Calidithermus chliarophilus* DSM 9957$^T$, and *Thermogemmatispora carboxidivorans* DSM 45816$^T$ were obtained from DSMZ (German Collection of Microorganisms and Cell Cultures, Braunschweig). *Deinococcus grandis* CCM 3997$^T$ and *Deinococcus aquatilis* CCM 7524$^T$ were obtained from the Czech Collection of Microorganisms (Masaryk University, Brno, Czechia).

Cells of *R. castenholzii* were grown anaerobically and aerobically. Anaerobic culture was grown in DSMZ medium 87 (*Chloroflexus aggregans* medium) under illumination with a halogen lamp at 48 XXXC. Aerobic culture was grown in a modified PE medium [23] in an Erlenmeyer flask at 48 XXXC with shaking (200 rpm) in the dark. Composition of the PE medium (pH 7.5–7.7): 0.38 g $l^{-1}$ $KH_2PO_4$, 0.39 g $l^{-1}$ $K_2HPO_4$, 0.50 g $l^{-1}$ $(NH_4)_2SO_4$, 0.10 mg $l^{-1}$ Vitamin $B_{12}$ (V6629-100MG, Sigma-Aldrich), 5 ml $l^{-1}$ basal salt solution, 10 ml $l^{-1}$ BME vitamin mixture (B6891, Sigma-Aldrich), 4.00 g $l^{-1}$ yeast extract. Composition of the basal salt solution: 24.65 g $l^{-1}$ $MgSO_4{\cdot}7H_2O$, 23.40 g $l^{-1}$ NaCl, 2.94 g $l^{-1}$ $CaCl_2{\cdot}2H_2O$, 1.11 g $l^{-1}$ $FeSO_4{\cdot}7H_2O$, 84.10 mg $l^{-1}$ $MnSO_4{\cdot}H_2O$, 28.80 mg $l^{-1}$ $ZnSO_4{\cdot}7H_2O$, 29.20 mg $l^{-1}$ $Co(NO_3)_2{\cdot}6H_2O$, 25.20 mg $l^{-1}$ $CuSO_4{\cdot}5H_2O$, 24.20 mg $l^{-1}$ $Na_2MoO_4{\cdot}2H_2O$, 31.00 mg $l^{-1}$ $H_3BO_3$, and 4.73 g $l^{-1}$ EDTA disodium salt dihydrate.

Cells of *T. carboxidivorans* were grown in a modified DSMZ Medium 592 in an Erlenmeyer flask at 55 XXXC with shaking (200 rpm) in the dark. The medium composition (pH 6.0): 1.30 g $l^{-1}$ $(NH_4)_2SO_4$, 0.25 g $l^{-1}$ $MgSO_4{\cdot}7H_2O$, 0.28 g $l^{-1}$ $K_2HPO_4$, 0.07 g $l^{-1}$ $CaCl_2{\cdot}2H_2O$, 0.02 g $l^{-1}$ Fe $Cl_3{\cdot}6H_2O$, 1 g $l^{-1}$ yeast extract, 1 g $l^{-1}$ tryptone, 1 ml $l^{-1}$ SL-8 trace elements solution. Composition of SL-8 trace elements solution: 36 mg $l^{-1}$ $Na_2MoO_4{\cdot}2H_2O$, 24 mg $l^{-1}$ $NiCl_2{\cdot}6H_2O$, 17 mg $l^{-1}$ $CuCl_2{\cdot}2H_2O$, 190 mg $l^{-1}$ $CoCl_2{\cdot}6H_2O$, 62 mg $l^{-1}$ $H_3BO_3$, 100 mg $l^{-1}$ $MnCl_2{\cdot}4H_2O$, 70 mg $l^{-1}$ $ZnCl_2$, 1.5 g $l^{-1}$ $FeCl_2{\cdot}4H_2O$, 5.2 g $l^{-1}$ EDTA disodium salt dihydrate.

Cells of *C. chliarophilus* were grown in the DSMZ-recommended Castenholz medium in an Erlenmeyer flask at 50 XXXC with shaking (200 rpm) for 3 days. The medium composition (pH 8.0) was: 100 mg $l^{-1}$ Nitrilotriacetic acid (Titriplex I), 60 mg $l^{-1}$ $CaSO_4{\cdot}2H_2O$, 100 mg $l^{-1}$ $MgSO_4{\cdot}7H_2O$, 8 mg $l^{-1}$ NaCl, 103 mg $l^{-1}$ $KNO_3$, 689 mg $l^{-1}$ $NaNO_3$, 140 mg $l^{-1}$ $Na_2HPO_4$ $\cdot 2H_2O$, 0.47 mg $l^{-1}$ $FeCl_3{\cdot}6H_2O$, 2.20 mg $l^{-1}$ $MnSO_4{\cdot}H_2O$, 0.50 mg $l^{-1}$ $ZnSO_4{\cdot}7H_2O$, 0.50 mg $l^{-1}$ $H_3BO_3$, 25 $\mu$g $l^{-1}$ $CuSO_4{\cdot}5H_2O$, 25 $\mu$g $l^{-1}$ $Na_2MoO_4{\cdot}2H_2O$, 46 $\mu$g $l^{-1}$ $CoCl_2{\cdot}6H_2O$, 1 g $l^{-1}$ tryptone, 1 g $l^{-1}$ yeast extract.

Cells of *D. grandis* were grown in PYE medium in an Erlenmeyer flask at 30 XXXC with shaking (200 rpm) in the dark. Composition of PYE medium (pH 7.2): 10 g $l^{-1}$ yeast extract, 10 g $l^{-1}$ peptone, 5 g $l^{-1}$ NaCl.

Downloaded from https://academic.oup.com/ismej/article/20/1/wrag021/8471199 by guest on 16 March 2026

Cells of *D. aquatilis* were grown in R2A medium (prepared according to manufacturer recommendation. NCM0188A, NEOGEN) in an Erlenmeyer flask at 30 XXXC with shaking (200 rpm) in the dark.

## Sampling hot spring mats

We organised two sampling campaigns to Rupite Hot Springs, Bulgaria (41.458310840335805, 23.2619133366458). During the first campaign on October 28th, 2021, we collected several cores from the local microbial mats (Fig. S1B, Supplementary material). The core samples were placed in cryovials and immediately stored in a dry shipper filled with liquid nitrogen. These snap-frozen samples were delivered frozen to the laboratory in Zürich and stored at −80 XXXC before subsequent experiments. Temperature and pH were measured using Multi 350i meter (WTW, Germany). Basic characteristics of the sampling sites are provided (Supplementary material, Table S1). During the second campaign on August 7th, 2023, we collected large fragments of the mats which were maintained at ambient temperature and delivered to the laboratory within 8 h and then kept at 46 XXXC with illumination by halogen lamp overnight before processing. Samples were collected at 15:00–16:00 local time (under clear sky conditions) in both sampling campaigns.

## DNA extraction

The samples were loaded into tubes with Lysis matrix A (MP Biomedicals) and disintegrated using FastPrep-24 5G (MP Biomedicals) equipped with QuickPrep Sample Holder (MP Biomedicals) with the following parameters: Speed = 7.0 m/sec, time = 45 sec, cycles = 1. The homogenised samples were resuspended in 470 $\mu$l TE buffer (50 mM Tris pH 8.0, 100 mM EDTA) supplied with 5 $\mu$l of 10 mg ml$^{-1}$ RNAse A (10 109 169 001, Sigma-Aldrich) and 25 $\mu$l of 10% sodium dodecyl sulfate. The tube was inverted 5–10 times by hand after each chemical was added to mix the solution. The mixture was incubated at 37 XXXC for 13 min. After incubation 7 $\mu$l of 18.5 mg ml$^{-1}$ Proteinase K (03115887001, Sigma-Aldrich) were added, and then the mixture was incubated at 37 XXXC for 1 h. After incubation, 100 $\mu$l of 5 M NaCl were added and mixed. Then 80 $\mu$l of the CTAB solution (10% Cetrimonium bromide, 0.7 M NaCl) were added. The mixture was incubated at 65 XXXC for 10 min. After the mixture cooled to room temperature, 700 $\mu$L of chloroform was added and mixed manually. The obtained emulsion was centrifuged at 20 000 × g for 10 min at room temperature. The upper aqueous phase was transferred to a clean tube. The procedure was repeated with 600 $\mu$l of chloroform. Isopropanol (0.6 V of the final volume) was added to precipitate DNA from the aqueous solution. DNA was pelleted by centrifugation at 10 000 × g for 10 min at room temperature. The pellet was washed in cold 70% ethanol, dried at room temperature, and dissolved in 60 $\mu$l of EB buffer (10 mM Tris, pH 8.5). After incubation at 37 XXXC for 30 min and mixing, the DNA solution was stored at −20 XXXC.

## 16S rRNA gene amplicon analysis

The amplification of the V3-V4 region of 16S rRNA gene, library preparation, and amplicon sequencing were done by Azenta Life Sciences (first sampling campaign) and Microsynth AG (second sampling campaign). Azenta Life Sciences employed proprietary PCR conditions and primers; sequencing was performed on a MiSeq System (Illumina) in 2x250 bp paired-end configuration. Microsynth AG employed standard 16S rRNA gene primers 341F/805R [24], two-step PCR library, and a NovaSeq System (Illumina) in 2x250 bp single-end configuration. Raw reads were quality-checked using FastQC v0.11.7 (Babraham Bioinformatics, Cambridge, UK). Subsequent analyses were done in R studio v3.6.1. The primer sequences were trimmed and read quality-filtered using Cutadapt v1.16 maximum error (−e 0.1), quality cut-off (−q 20) and minimum length (−m 250) [25]. Reads were truncated using *filterAndTrim* (truncLen = c(225, 225), maxEE = c(2,5), truncQ = 2) in the R/Bioconductor environment from DADA2 package v1.12.1 [26]. ASVs were constructed and chimeric sequences removed using the method "pooled." Additional chimeric sequences were removed by selecting 370–430 bp length range. Taxonomic assignment of amplicons was performed using non-redundant SILVA r138.1 16S rRNA gene database using *dada2:assignTaxonomy*. To reduce singletons and doubletons, reads found less than 3 times in less than 20% of the samples were removed from subsequent analysis. Community composition barplots were generated using Phyloseq v1.30.0 [27] and ggplot2 v3.3.6 [28].

## Metagenomic analysis

Metagenomic sequencing of the mat DNA was done using NEBNext Ultra II FS DNA Library Prep Kit and a NovaSeq S1 System (Illumina) in 2x150 bp paired-end configuration. Raw reads from three metagenomes (green, yellow, and red mat) were quality-filtered and adapters removed using Trimmomatic v0.36 (LEADING:3 TRAILING:3 SLIDINGWINDOW:4:15 HEADCROP:9 MINLEN:100) [29], and reads were assembled using SPAdes v3.13.1 [30] (following kmers 21,33,55,77 127 –meta parameters). Obtained contigs (>2.5 kb) were used for binning with MetaBAT2 2.12.1 with default parameters [31]. CheckM [32] was used to estimate bin completeness and contamination. Poorly resolved bins with contamination >10% were further manually curated by removing contigs with different sequencing depths [33], which were calculated according to previous method [34], and with repeated rounds of contamination/completeness assessment by CheckM. Final curated bins with completeness >50% and contamination <10% were considered MAGs. They were further taxonomically classified using GTDB-tk [35] (Supplementary material, Table S2). In total 35 MAGs were assembled, 12 MAGs from the yellow layer, 9 from the green layer, and 14 from the red layer. Accession numbers of MAGs are provided (Supplementary material, Table S2). Taxonomic annotation of the shotgun reads was done using kaiju with database kaiju_db_nr_2023–05–10 [36].

## Identification of sheath genes in metagenomic data and recruitment analysis

Two MAGs, one from green mat, and one from yellow mat were classified as *Roseiflexus* sp. Based on ANI/AAI analysis done using fastANI [37] and AAI: Average Amino acid Identity calculator [38] they represent the same species with 99.9 and 99.75% of identity, respectively. Both of the MAGs were annotated using Prokka [39] and analysed in Geneious Prime 2023.2. to obtain the CIS cluster.

All three metagenomes were checked for the presence of any other sheath gene from non-redundant database consisting of 1679 sheath gene sequences which were downloaded as sequences with annotation "afp2/3/4" from previously created online eCIS database [15]. Fragment recruitment was used to assess abundances of MAGs in the metagenome. Metagenomic reads were mapped against the MAGs using BLASTn with a cutoff of 70% query coverage, *e*-value 0.1, and

Downloaded from https://academic.oup.com/ismej/article/20/1/wrag021/8471199 by guest on 16 March 2026

the "best hit" option. Finally, abundances were calculated considering only the hits with identities ≥95%. To compare abundance across the distinct metagenomes, the number of recruited bases from the mapped reads was normalized by the total size of each metagenome (expressed as base pairs per megabase of the metagenome).

## Sample vitrification

Frozen mat samples from the first sampling campaign were thawed at room temperature. Small pieces were cut from the mat samples using a sterile scalpel and then softly homogenised into a cell suspension using a sterile glass mortar and pestle. The cell suspension was subsequently vitrified using a Vitrobot Mark IV System (Thermo Fisher Scientific Inc., USA) [40]. Briefly, we applied 4.5 and 3.5 $\mu$l of the cell suspension (first and second sampling campaigns, respectively) to glow-discharged copper electron microscopy (EM) grids (R2/2 and R2/1 H2, Quantifoil). The EM grids were then back-blotted for 5 or 9 s in the humidified (100%) Vitrobot chamber and plunged into liquid ethane-propane (37/63 Mol%/Mol%). Finally, the grids were stored in liquid nitrogen until further processing. The back-blotting was carried out using filer paper from the back of the grid and a Teflon sheet at the front. Cells from the bacterial cultures were frozen using the same procedures and materials.

## Cryo-focused ion beam milling

All lab cultures and the mat samples from the second sampling campaign were cryoFIB milled following the automated sequential FIB milling scheme previously described in [41]. A Crossbeam 550 FIB-SEM instrument (Carl Zeiss AG, Germany) was used, equipped with a copper-band cooled mechanical cryo-stage (Leica Microsystems GmbH) and an integrated VCT500 vacuum transfer system (Leica Microsystems). In short, frozen EM grids were loaded onto a pre-tilted cryo-holder in a VCM loading station (Leica Microsystems) and transferred to an ACE600 (Leica Microsystems) using the VCT500. The grids were coated with 4–7 nm of Tungsten before being inserted into the Crossbeam. In the Crossbeam, an additional layer of organoplatinum was applied. Scanning electron microscopy with the SE2 and in-lens secondary electron detectors (Carl Zeiss AG, Germany) was then used to determine grid quality (3–10 V, 58 pA) and to target cells (3 V, 58 pA). Using automated sequential FIB milling, lamellae of ~250 nm thickness were generated at a milling angle of 12XXX-15XXX. Targets were sequentially milled using 700 pA, 300 pA, and 100 pA for rough milling and 50 pA for polishing. Once milling was completed, the cryo-holder was transferred to the VCM loading station using the VCT500 where the grids were unloaded and stored in liquid nitrogen until further processing.

## CryoET data collection and processing

CryoET data were collected using a Titan Krios G4 cryo-electron microscope (Thermo Fisher Scientific Inc., USA) with an accelerating voltage of 300 kV. The microscope was equipped with a BioContinuum imaging filter and a K3 direct electron detector (Gatan). Tilt series were acquired using SerialEM [42, 43] and PACE-tomo [44] following bidirectional or dose-symmetric tilt schemes with 2° or 3° increments at −8 $\mu$m defocus. For non-FIB-milled bacterial cells, the tilt series were collected over a range from −60° to +60° with a total electron dose of ~159 $e^-/Å^2$ and pixel size of 4.51 Å. To account for the pre-tilt, lamellae of cryoFIB-milled cells were imaged over a range from −50° to +70° with a total electron dose of 82–140 $e^-/Å^2$ and pixel size of 4.51 Å.

The tilt series were drift-corrected using the alignframes command in IMOD [45]. Cryo-tomograms were reconstructed using IMOD with the back projection method and 4× binning. The tomograms were CTF-deconvolved and filtered using IsoNet to improve contrast [46]. Dragonfly was used to segment tomograms according to the published protocol [47]. UCSF ChimeraX was used to visualize the results of the segmentations [48].

## Isolation of CIS particles from bacterial cells and room temperature-TEM

To isolate CIS particles from bacterial cells, pelleted bacterial cultures or fragments of microbial mats were placed into 2 ml tubes with Lysing Matrix A (116910050-CF, MP Biomedicals). The mat fragments were prepared by sectioning the core samples into three layers according to the color of the mat material: yellow, green, and red. The samples and Lysing Matrix A were supplied with 1 ml of cold sample buffer (150 mM NaCl, 50 mM Tris, pH 7.4, 2x cOmplete, EDTA-free Protease Inhibitor Cocktail) and bead-beaten in FastPrep-24 5G (MP Biomedicals) using QuickPrep Sample Holder (MP Biomedicals) at 4 XXXC with the following parameters: Speed = 7.0 m $s^{-1}$, time = 45 sec, cycles = 1. The homogenate was mixed with lysis buffer (150 mM NaCl, 50 mM Tris, pH 7.4, 300 $\mu$g $ml^{-1}$ lysozyme (62971-10G-F, Sigma-Aldrich), 60 $\mu$g $ml^{-1}$ DNAse I (10 104 159 001, Sigma-Aldrich), 0.5x Protease Inhibitor Cocktail), and incubated at 37 XXXC for 15 min. Cell debris was removed by centrifuging the lysed material at 15 000 × g for 15 min at 4 XXXC. The CIS particles were pelleted by ultracentrifugation at 150 000 g for 1 h at 4 XXXC and resuspended in the cold sample buffer.

To image CIS particles, the preparations were applied to glow-discharged, formvar-coated copper grids (FCF200-CU 50/pk, Formvar/-Carbon 200 Mesh) for 60 s, and stained twice with 1% phosphotungstic acid. The stained grids were analysed at room temperature using transmission electron microscope Morgagni 268 (Thermo Fisher Scientific Inc., USA) operated at 80 kV.

## Protein identification in the CIS preparations

Proteins in samples with isolated CIS particles were identified at the Functional Genomic Center Zurich. Briefly, proteins were precipitated from the CIS preparations by adding trichloroacetic acid (Sigma-Aldrich) to a final concentration of 5% and subsequently washed twice with ice-cold acetone. The pellet was air-dried and dissolved in a buffer (10 mM Tris, 2 mM $CaCl_2$, pH 8.2). Then, proteins were reduced and alkylated by adding Tris (2-carboxyethyl) phosphine and 2-chloroacetamide to a final concentration of 5 mM and 15 mM, respectively. The samples were incubated for 30 min at 30 XXXC light protected. Then, samples were enzymatically digested with trypsin (pH 8) and dried. Peptides were acidified to perform a cleanup using home-made C18 stage-tips (peptides were loaded on the tip, washed, eluted, and dried). The digested samples were dissolved in aqueous 3% acetonitrile with 0.1% formic acid. Peptides were separated on a M-class UPLC and analysed on a Ion Trap mass spectrometer (Thermo Fisher Scientific Inc., USA). The acquired MS data were processed for identification using PEAKS Studio XPlus (Bioinformatic Solutions). Spectra were searched against custom proteome database (generated from our metagenomic contigs longer than 1 kb), concatenated to

Downloaded from https://academic.oup.com/ismej/article/20/1/wrag021/8471199 by guest on 16 March 2026

its reversed decoyed fasta database. Methionine oxidation was set as variable modification, Carbamidomethyl (C) as fix modification. Enzyme specificity was set to trypsin allowing a maximum of two missed-cleavages. A fragment ion mass tolerance of 0.02 Da and a parent ion tolerance of 10 ppm were set. Scaffold 5.3.3. (Proteome Software Inc., version 5.10) was used to validate MS/MS based peptide and protein identifications. Peptide identifications were accepted if they achieved a false discovery rate (FDR) of less than 0.1% by the Scaffold Local FDR algorithm. Protein identifications were accepted if they achieved an FDR of less than 1.0% and contained at least 2 identified peptides. Comprehensive details of the sample processing protocol can be found in the supplementary material.

### Immunogold labelling

5 $\mu$l of CIS preparations were applied on glow-discharged EM grids (FCF200-CU-50, Electron Microscopy Sciences) and incubated for 2 h at room temperature in a closed Petri dish with water in a smaller dish inside to prevent fast drying. The grid was washed with cold sample buffer and blocked with filtered 0.1% bovine serum albumin (A7030-50G, Sigma-Aldrich) for 1 h at room temperature. Then the grid was washed again and incubated overnight at 4 XXXC with custom polyclonal *Roseiflexus*-specific anti-sheath antibodies (diluted 1:50) or rabbit IgG control (A01008, GenScript). Then the grid was washed again and incubated for 2 h at room temperature with gold-conjugated anti-rabbit secondary antibodies (Sigma-Aldrich, code G7277-.4ML). Finally, the grid was washed, dried at room temperature, and stained with 1% phosphotungstic acid before being imaged on the TEM Morgagni 268 operated at 80 kV. All washing steps were done in a 1.5 ml tube with 500 $\mu$l of the cold sample buffer. The grid was blotted with blotting paper between washing and incubations. The tube was turned 5 times and incubated for 10–20 min at room temperature to complete washing. The number of labelled CIS (sheath) particles and the total number of CIS particles were manually counted in images randomly collected from areas on the EM grids. We analysed 56 images for preparations from mat layers and 52 image for preparations from axenic cultures of *R. castenholzii* and *S. coelicolor*. Average number of the labelled CIS particles and average number of the total number of CIS particles were calculated by analysis of three independent mat cores. A CIS particle is classified as labelled if it is covered by at least four gold beads. One-way ANOVA followed by multiple comparison Šidák test was performed using GraphPad Prism version 10.5.0.

The *Roseiflexus*-specific anti-sheath antibodies were generated to target a sheath protein epitope exposed on outer surface of the assembled sheath particle. Since structure of the sheath protein from *Roseiflexus* bacteria was not available, we first found the exposed epitope in the cryo-EM structure of the contracted sheath proteins from *S. coeilicolor*, which is the phylogenetically closest protein with resolved structure [10]. This epitope was in domain 3. Second, we aligned sequences of the sheath protein from *Roseiflexus* genomes with the sheath sequence from genome of *S. coeilicolor* and selected locus homologues to domain 3 (Supplementary material, Fig. S2). The sequence from the *R. castenholzii* genome in this locus was used for the generation of the anti-sheath rabbit antibodies by GenScript (PolyExpress package SC1676). The target sequence was: GKAPPPPRLELPTRASKALTSLIVTPKSETASDIQVEIGPPVGENPP-PEAFTVKISMGEVKEVYENVSFNKRPKDGTSYVVEKINSSSTLVQVAEGPA TGSLADRVPEFGMSVIKPLAPIVPARVDATTFVGSAAERS.

### Phylogenetic analysis of the CIS proteins

We used sequences of the baseplate (WP_012121309.1) and sheath (WP_012121318.1) proteins from *R. castenholzii* DSM13941 as query sequences for PSI-BLAST (blast.ncbi.nlm.nih.gov) search against all non-redundant GenBank CDS. Multiple protein sequence alignment was constructed using MAFFT with L-INS-I parameter (–-inputorder –maxiterate 1000 –retree 1 –localpair input) [49]. Phylogenetic tree was calculated using IQ-TREE 1.6.11 [50] with the LG + F + I + G4 model recommended by ModelFinder [51] and branch supports were estimated using UFBoot2 [52]. The calculated phylogenetic tree was visualized using iTOL [53].

## Results

### Rupite Hot Springs mats accommodate a substantial Roseiflexus population

We collected microbial mats from the Rupite Hot Spring, which is known to accommodate a population of *Roseiflexus* [54, 55]. After the first sampling campaign, we extracted genomic DNA from the snap-frozen mat samples and conducted 16S rRNA gene amplicon sequencing, which confirmed the presence of a substantial population of *Roseiflexus* bacteria (5.4%–61.0%) in the samples from the high-temperature sites (>48 XXXC) of the hot spring (Fig. S1, Table S1, Supplementary material).

### Environmental cryoET reveals an intracellular CIS in Roseiflexus-like cells

As an initial step in our cryoET approach to environmental samples, we examined the condition of mat cells after recovery from their snap-frozen state. Recovered mat samples were gently homogenised, plunge-frozen, and screened by cryoET. This revealed that cells had lost their integrity (Supplementary material, Fig. S3). Therefore, we collected new mat samples and delivered them from the sampling site (Fig. 1A) to our workflow without snap-freezing to minimise the loss of cellular integrity.

We cut small fragments from the fresh mat samples, gently homogenised them to generate a cell suspension, and split the suspensions into aliquots for further cryoET analysis and DNA extraction (Fig. 1B). The genomic DNA was used to conduct 16S rRNA gene amplicon sequencing, which was an important step in our workflow, because it generated a list of the bacteria present in the mat samples. We found that within the top 10 bacterial genera present in the mat, *Roseiflexus* bacteria were the only bacteria with known filamentous multicellular morphology and without thylakoids, and chlorosomes (Fig. 1C). The genus *Roseiflexus* contributed 13% and 42% of the total reads in sample 1 and sample 2, respectively. Therefore, we expected a high abundance of *Roseiflexus* cells in the mat material frozen on EM aliquoted for further cryoET imaging.

To acquire environmental cryoET data, we plunge-froze the mat cell suspensions on EM grids. Cryogenic scanning electron microscopy (cryoSEM) of the EM grids revealed a relatively thin layer of the mat cells (Fig. 1D), which was only achieved due to a homogenisation step prior to plunge-freezing. A relatively thin layer of the sample is essential for sample vitrification, since plunge-freezing is limited by sample thickness [56]. Additionally, the thin sample layer allowed for automated cryoFIB milling of the mat cells allowing us to generate 34 thin lamellae from the bulk material of the frozen mat cells.

Downloaded from https://academic.oup.com/ismej/article/20/1/wrag021/8471199 by guest on 16 March 2026

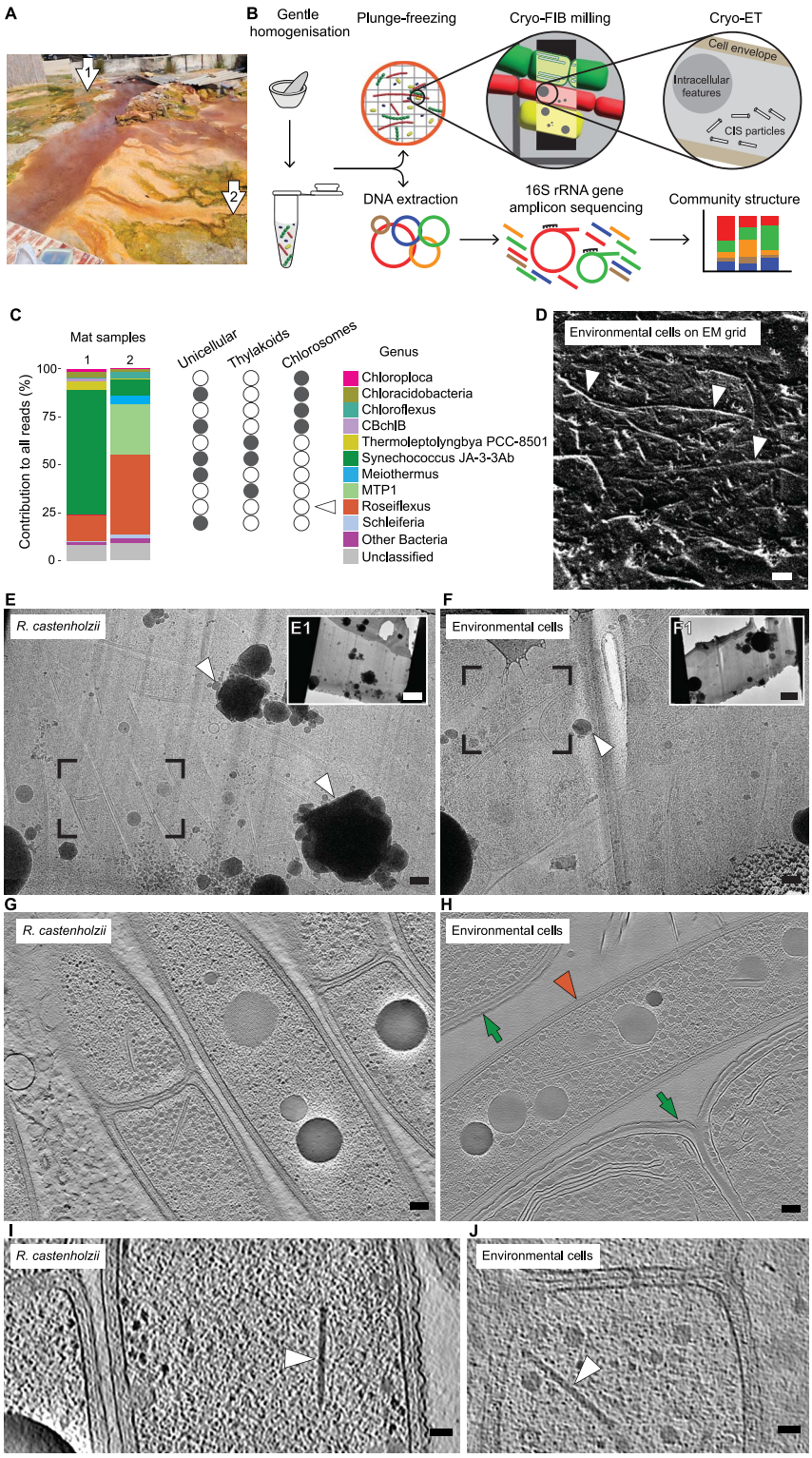


**Figure 1** Environmental cryoET unveils intracellular CIS in the mat cells. (A) Rupite hot spring during second sampling campaign. Arrows point to the sampling site. (B) Scheme showing the workflow for environmental cryoET. (C) The bar plot shows the relative abundance of *Roseiflexus* among the top 10 bacterial genera according to 16S rRNA gene amplicon sequencing results. The circles show presence (grey) and absence (white) of the morphological traits. Arrowhead points on traits of *Roseiflexus* bacteria. (D) CryoSEM image shows mat cells (arrowheads) on surface of EM grid. (E) Cryo-TEM image shows lamella milled through aerobic R. castenholzii cells. Full overview of lamella is shown in the right top incretion (E1). The box indicates the area used to collect cryoET data, which were then reconstructed into the cryo-tomogram shown in G. The arrowhead indicates ice contamination. (F) Cryo-TEM image shows milled lamella of mat homogenate on an EM grid. Full overview of lamella is shown in the right top incretion (F1). The box indicates the area used to collect cryoET data which were then reconstructed into the cryo-tomogram shown in H. The arrowhead indicates ice contamination. (G) Slice through a cryo-tomogram shows aerobic R. castenholzii cells. (H) Slice through cryo-tomogram shows cyanobacterial (green arrows) and *Roseiflexus*-like cells (orange arrowhead) from the mat. (I/J) Slices through cryo-tomograms of R. castenholzii (I) and environmental *Roseiflexus*-like cells (J) show CIS-like intracellular features (arrowhead). Slice thickness: 18 (G, H, I) and 13.5 (J) nm. Scale bars: D 10 $\mu$m; E, F 300 nm; E1, F1 2 $\mu$m; G, H 100 nm; I, J 50 nm.

Downloaded from https://academic.oup.com/ismej/article/20/1/wrag021/8471199 by guest on 16 March 2026

Guided by the list of the bacterial species in the sample (Fig. 1C), we searched the *Roseiflexus*-like morphotypes (filamentous multicellular bacteria without thylakoids and chlorosomes) in our images. In parallel, to improve the confidence in targeting *Roseiflexus* cells in the mat lamellae, we cryoFIB-milled lamellae of cells from axenic cultures of *R. castenholzii* (reference lamellae). Images of *R. castenholzii* cells in the reference lamellae (Fig. 1E) were used to identify *Roseiflexus*-like cells and select priority areas in the mat lamellae for data acquisition (Fig. 1F). However, to better understand the cellular composition of the entire mat, we collected cryoET data in areas with and without potential *Roseiflexus* cells, resulting in 89 cryo-tomograms.

To identify *Roseiflexus*-like cells in the cryo-tomograms, we collected reference cryo-tomograms on lamellae cryoFIB-milled through anaerobic (19 cryo-tomograms) and aerobic (71 cryo-tomograms) axenic culture of *R. castenholzii* (Fig. 1G). We then catalogued the cellular features of *R. castenholzii*. These features included regularly organised sheets, flat membranous intracellular features, vesiculations of the cell membrane, septal channels, and putative polyhydroxyalkanoate-, polyphosphate-, and glycogen granules (Supplementary material, Fig. S4). Organisation of the cell envelope, especially at the cell–cell junction, was also used as an important feature characterising *Roseiflexus* cells.

When examining the mat cryo-tomograms, we utilised the catalogue of *Roseiflexus* cellular features to confirm that the cells we targeted in the lamellae were indeed *Roseiflexus*-like cells (Fig. 1H). Overall, we found 33 environmental *Roseiflexus*-like cells in our mat cryo-tomograms.

While analysing cryo-tomograms of *R. castenholzii* cells and *Roseiflexus*-like cells from the mat, we found intracellular rod-like features (Fig. 1I/J). In both *R. castenholzii* and mat cells, the CIS-like particles were freely deposited in the cytoplasm without any anchoring to the cell envelope, resembling an extended form of eCIS/cCIS [6, 10]. These CIS-like particles were absent in tomograms of *R. castenholzii* cells from anaerobic cultures (Supplementary material Fig. S5). All CIS-like particles in aerobically grown *R. castenholzii* cells were extended and had the average length of 217±16 nm (n = 218). In the mat dataset, we found up to 12 examples of the *Roseiflexus*-like cells with extended and contracted intracellular CIS-like particles (Fig. 1J, Supplementary material, Fig. S6). The average length of the extended particles in the mat cells was 251±26 nm (n = 14).

To conclude, cryoFIB/cryoET techniques guided by 16S rRNA gene amplicon sequencing enabled us to visualize bacterial cells collected directly from the natural environment and discover a putative eCIS/cCIS-like protein complex in these cells.

## Roseiflexus cells are a major contributor to the CIS pool of the microbial community

Although we used cryoET to show the presence of CIS in environmental *Roseiflexus* cells *in situ*, we aimed to put the *Roseiflexus* CIS into the context of the whole *Roseiflexus* population and into the context of the microbial mat community. Therefore, we applied a holistic approach to the snap-frozen multi-layered mat samples (first sampling campaign) in order to analyse the distribution of putative CIS genes in the microbial community. The mat was dissected into red, green, and yellow layers (Fig. 2A). We assumed that every layer represented a specific micro-niche in the mat community because every layer was dominated by differently pigmented microorganisms.

To identify all potential CIS-producers in the mat, we conducted shotgun sequencing of DNA from the mat layers and discovered all bacteria with CIS genes in the microbial community (Fig. 2A). Taxonomic assignment of the reads showed that *Roseiflexus* and cyanobacteria were the dominating bacterial genera (Fig. 2B). We assembled, translated, and annotated the metagenome from our DNA sequencing dataset, resulting in the metagenome of the mat and a set of metagenome-assembled genomes (MAGs) with completeness >50% and contamination <10% (Supplementary material, Table S2). *Roseiflexus* MAGs were assembled from the green and yellow layers but not from the red layer, even though *Roseiflexus* sp. is the most abundant bacterium in this layer. This occurred probably due to the high strain diversity of the *Roseiflexus* population within the red layer. The high microdiversity of co-occurring abundant microbial species is likely to generate assembly problems and reducing the quality of metagenome assembly [57].

We lysed the mat cells and pelleted all large macromolecular complexes from the layers to purify CIS particles. Again, as for environmental cryoET, we used an axenic aerobic culture of *R. castenholzii* as a reference sample. We found similar empty contracted CIS-like (sheath) particles in all preparations from the reference sample and from each of the mat layers (Fig. 2C). To identify the proteins in these preparations, we performed mass spectrometry with peptide search against all our metagenomic contigs longer than 1 kb. The search resulted in 182 proteins being identified in the mat layers with 68 proteins being annotated as hypothetical proteins (Supplementary material, Fig. S7, Table S3). Using a BLASTp search against GenBank, we found sheath proteins among those hypothetical proteins. Additionally, we found cyanophage-related proteins encoded in *Elainellaceae* MAG (former *Leptolyngbya* sp. O-77) (Supplementary material, Table S4).

The sheath genes were found in the contigs that assigned to *Roseiflexus* sp., *Thermaurantiacus* sp., and *Aggregatilineales* sp. MAGs. CIS proteins are typically encoded by genes that are organized as a gene cluster on the bacterial chromosome or plasmid [15]. Using BLASTn search, we found other CIS-related genes down- and upstream of the sheath genes and assigned this locus as the *Roseiflexus* CIS gene cluster (Fig. 2D). We also found CIS gene clusters in *Thermaurantiacus* and *Aggregatilineales* MAGs (Fig. 2D). The *Roseiflexus* MAGs encoded all structural CIS genes predicted previously in the genome of *R. castenholzii* [15, 16], but dispersed in multiple contigs in the MAGs (Fig. 2D). We mapped the metagenomic reads to the three MAGs and found that *Roseiflexus* was the most abundant of these organisms and potentially the major contributor to the CIS pool in the red and green layers (Fig. 2E).

To confirm that *Roseiflexus* is the major contributor to the mat CIS pool, we developed an immuno-TEM protocol and designed anti-sheath antibodies for the identification and quantification of *Roseiflexus* CIS particles (see Methods). The anti-sheath antibodies were applied as primary antibodies to the CIS preparations from *R. castenholzii* and *S. coeilicolor*, which we considered as positive and negative controls, respectively. Anti-rabbit gold-conjugated secondary antibodies were applied to the CIS preparations after incubation with anti-sheath antibodies and resulted in labelling of 99.2% and 0.3% of particles in positive and negative controls, respectively (Supplementary material Fig. S8). Also, we validated a relatively low rate of unspecific binding by secondary antibodies in the absence of the primary antibodies but in the presence of rabbit IgG control (Supplementary material Fig. S8).

Downloaded from https://academic.oup.com/ismej/article/20/1/wrag021/8471199 by guest on 16 March 2026

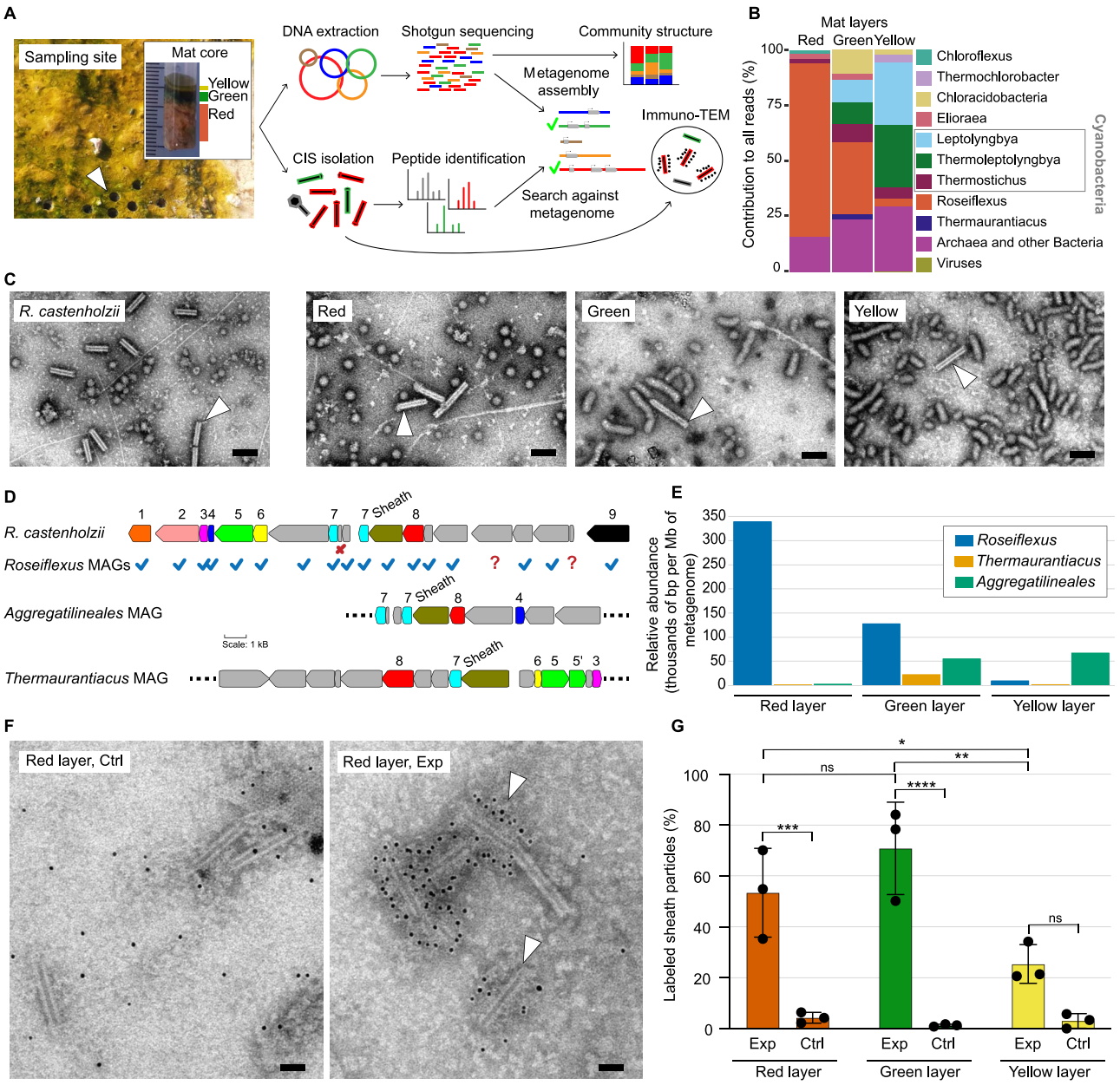


**Figure 2** *Roseiflexus* population is a major contributor to the mat CIS pool. (A) Scheme showing the workflow from collecting mat cores (top left image) to metagenome assembly and immuno-TEM. (B) The bar plot shows the relative abundance of *Roseiflexus* among the top 10 microbial species, based on the taxonomic annotation of shotgun reads using Kaiju. (C) TEM images show CIS (sheath) particles purified from an R. castenholzii axenic culture and each of the mat layers. Arrowhead points at the contracted CIS (sheath) particles. (D) The scheme shows the CIS gene cluster of R. castenholzii (used as reference) and the CIS gene locus in the Rupite MAGs (check mark = presence of a gene, x = gene was not present in the locus,? = gene was not found). The numbers correspond to gene annotations: 1, 2, 3, putative baseplate genes; 4, 5, 6, putative spike genes; 7, inner tube gene; 8, putative apical cap gene; 9, ATPase gene. (E) The bar plot shows relative abundance of *Roseiflexus* sp., *Thermaurantiacus* sp., and *Aggregatilineales* bacterium from the different mat layers calculated based on normalized read mapping (the number of base pairs [bp] per megabase [Mb] of metagenome). (F) TEM images show examples of labelled CIS particles (arrowhead) from the mat samples. (G) Bar plot showing the distribution of the labelled CIS particles in the mat samples. Primary anti-sheath rabbit antibodies were applied for labelling the sheath (Exp). Rabbit IgG control was applied as control to check the unspecific binding of anti-rabbit gold-conjugated secondary antibodies (ctrl). The fraction of labelled CIS particles in both experimental and control conditions was calculated as the average of three independent replicates (Fig. S10). The numbers of labelled CIS particles and total CIS particles for each replicate and layer are reported in Supplementary Table S5. Statistical significance between the samples was assessed using ordinary one-way ANOVA followed by multiple comparison Šidák test. Multiplicity adjusted *P* value was reported [ns (not significant), 0.1234; *, 0.0332; **, 0.0021; ***, 0.0002; ****, <0.0001]. Scale bars: C, 100 nm; F, 50 nm.

The anti-sheath antibodies labelled CIS (sheath) particles in preparations from the mat layers (Fig. 2F, Supplementary material Fig. S9). 53.4% and 70.9% of the particles were labelled in the red and green layers, respectively (Fig. 2G). The yellow layer had only 25.4% of the particles labelled. These average numbers of the labelled particles were calculated by analysis of three independent mat cores

Downloaded from https://academic.oup.com/ismej/article/20/1/wrag021/8471199 by guest on 16 March 2026

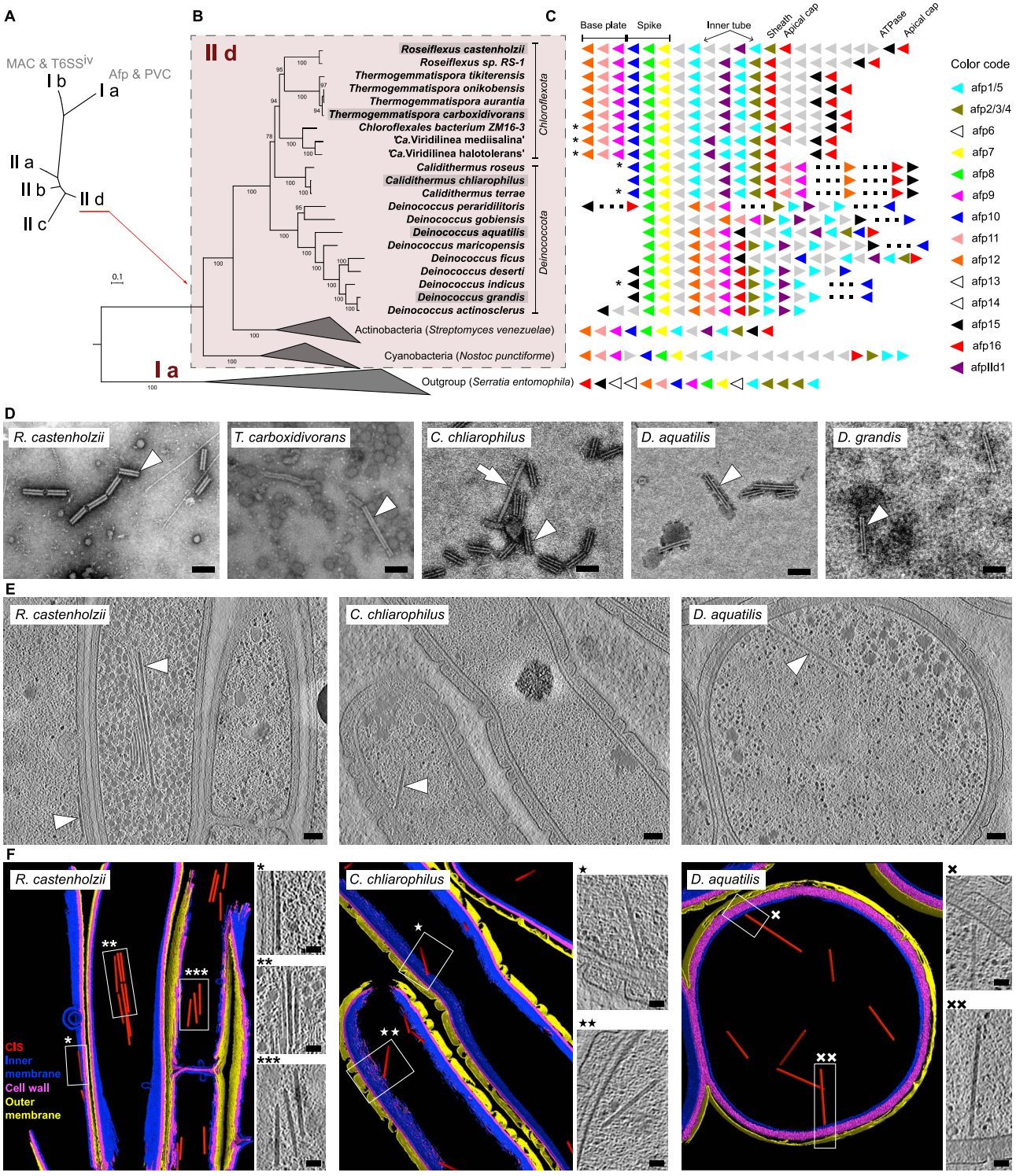


**Figure 3** *Roseiflexus* CISs belong to a clade of cytoplasmic CISs from extremophilic bacteria. (A) Simplified scheme of the previously reconstructed phylogenetic tree [10]. The scheme shows eCIS lineages. (B) Maximum-likelihood phylogenetic tree showing a clade of *Roseiflexus*-related CISs. Scale bar shows number of substitutions per site. Version of the tree with expanded clades is shown in supplementary material (Fig. S11). The tree was reconstructed based on analysis of concatenated sheath and baseplate proteins. Grey highlighted strains were used for CIS preparations (shown in D). (C) Scheme shows an organisation of the CIS gene clusters in genomes from the *Roseiflexus* CIS clade, other members of CIS lineage subtype IId. Gene names were used as previously described [10]. Asterisk highlights draft genomes. Dashed line shows gaps between contigs. (D) TEM images showing CIS (sheath) particles purified from cells of the selected strains. Arrowhead points to the CIS particles. (E/F) Slices through cryo-tomograms (E) and corresponding models (F) showing the CIS particles (arrowhead/box) in cells of R. castenholzii, *C. chliarophilus*, D. aquatilis. Scale bars: D, E 100 nm; F (insertions), 50 nm.

Downloaded from https://academic.oup.com/ismej/article/20/1/wrag021/8471199 by guest on 16 March 2026

(Supplementary material Fig. S10, Table S5). The average length of the labelled particles in the green layer was 85.1 ± 9.6 nm (n = 124), which was close to the length of the particles in preparations from an aerobic axenic culture of *R. castenholzii* (86.7±7.0 nm, n = 175).

Despite the red layer containing at least twice the *Roseiflexus* population of the green layer, CIS particles from *Roseiflexus* cells comprise an equally large fraction of the CIS pool in the green layer as in the red layer. These results indicate that *Roseiflexus* cells in the green layer produce more CIS particles than those in the red layer. Thereby, combination of DNA sequencing method, protein mass spectrometry and immuno-TEM enabled us to discover a niche-specific expression of *Roseiflexus* CISs in the bacterial populations in their natural environment.

### The Roseiflexus CIS belongs to a clade of cytoplasmic CISs from extremophilic bacteria

In the presented work, *Roseiflexus* bacteria were the first confirmed CIS-producing thermophilic bacteria. Previously, hypothetical CISs from *R. castenholii* were placed into CIS lineage IId (Fig. 3A) together with cytoplasmic CISs from *Streptomyces* [15]. To characterise this system further, we searched for CIS gene clusters in other bacteria using the *Roseiflexus* sheath gene as a query for Position-Specific Iterated BLAST against the GenBank database (non-redundant protein sequences). We found CIS gene clusters in multiple genomes of bacteria belonging to *Chloroflexota* and *Deinococcota* phyla (Fig. 3B). Next, we reconstructed a maximum-likelihood phylogenetic tree based on the concatenated sheath and baseplate J-like protein (Afp11) proteins and found that these CISs indeed form a clade outside cytoplasmic CISs (*Streptomyces*) but within the clade IId (Fig. 3B). CISs from thermophilic *Deinococcota* strains clustered with *Chloroflexota* CISs but not with mesophilic *Deinococcota*. Additionally, the gene cluster organisation had higher similarity between *Chloroflexota* and thermophilic *Deinococcota* than between thermophilic and mesophilic *Deinococcota* (Fig. 3C). These results suggest an acquisition of the CIS gene cluster via horizontal gene transfer between *Streptomyces*, *Chloroflexota*, and *Deinococcota*.

To validate the assembly of CIS particles in cells of these *Chloroflexota* and *Deinococcota* strains, we selected representative strains and applied the CIS purification protocol to cell pellets obtained from their respective axenic cultures. *T. carboxidivorans* was a representative strain of thermophilic mycelial *Chloroflexota* species [58]. *C. chliarophilus* was a representative strain of thermophilic *Deinococcota* species [59, 60]. *D. aquatilis* and *D. grandis* were representative strains of mesophilic but UV/Gamma radiation-resistant *Deinococcota* species [59, 60]. All preparations retrieved contracted sheath with rare examples of extended CIS particles as we have previously observed in preparations from *R. castenholzii* (Fig. 3D). Next, we cryoFIB-milled the plunge-frozen cells of *C. chliarophilus* and *D. aquatilis* and imaged them with cryoET as representative examples of thermophilic and mesophilic *Deinococcota* in the CIS clade. In cryo-tomograms of these cells, we observed intracellular CIS particles (Fig. 3E and F). The *Deinococcota* CIS particles were localised unattached in the cytoplasm, similar to CIS localisation in *Roseiflexus* cells. The average length of the intracellular CIS particles was 238±14 (n = 69) and 365±39 (n = 20) for *C. chliarophilus* and *D. aquatilis*, respectively. In conclusion, we discovered that *Roseiflexus* CIS is a member of the CIS lineage i.e. expressed and assembled in extremophilic bacteria.

## Discussion

Multiple novel CIS have been discovered in bacteria and archaea by studying microbial cultures in recent years. However, it was often difficult to place these systems back into the context of their native microbial environment. In this work, we looked at the CIS discovery from a different angle using an approach based on a combination of conventional omics techniques with cryoFIB/cryoET to analyse microbial cells from their natural habitat. Although we targeted specific bacterial cells and relied on the reference cryoET data, our study shows that cryoET can be applied as a discovery tool in environmental microbiology.

Because we validated the CIS assembly in environmental *Roseiflexus* cells, we can conclude that this system plays a role in the lifestyle of this bacterium under natural conditions. Phylogenetically, *Roseiflexus* CIS belongs to the same lineage (subtype IId [15]) as the recently discovered cytoplasmic CIS in *Streptomyces*, which has a cytoplasmic mode of action and induces the cell lysis under stress conditions [10–12, 61]. Also, the CIS gene cluster in *Roseiflexus* genomes shares similarity regarding synteny with the CIS gene cluster in *Streptomyces* strains with validated function and was probably acquired via horizontal gene transfer between *Chloroflexota* and *Streptomyces*. Therefore, CIS in *Roseiflexus* bacteria may exhibit the cytoplasmic mode of action. This hypothesis is further supported by the unanchored intracellular localisation of the CIS particles in *Roseiflexus* cells and the CIS behaviour upon purification. All CIS preparations contained only contracted particles, suggesting CIS contraction upon cell lysis and low stability of the extended form, in contrast with the behavior of eCISs, which retain stability upon cell lysis in order to execute their function [6]. Additionally, intracellular contracted CIS particles were observed only in the lysed *Roseiflexus*-like cells from the mat (Fig. S6). Intact cells possessed only extended CIS particles in cells from both axenic culture and mat. Although the firing and potential membrane attachment of cCIS particles in *Streptomyces* requires the protein CisA [61], the mechanism may differ in *Roseiflexus* due to the absence of close *cisA* homologues. Unfortunately, no genetic system is currently available for *Roseiflexus* strains to generate a non-contractile sheath mutant, which would be crucial for the validation of the involvement of *Roseiflexus* CISs in cell death and life cycle regulation.

By studying cells directly collected from their natural environment, we discovered a niche-specific level of the CIS particle production. The high CIS production in the green layer may be linked to the cyanobacterial activity in this fraction of the mat community. The multi-layered organisation of the hot spring mats is thought to be formed as an adaptation of phototrophs (*Roseiflexus, Chloroflexus*, and cyanobacteria) to utilise different wavelengths of light and hence reduce competition for the energy source [19]. The niche-specific CIS production lets us consider a new element of intercellular interactions governing this spatially structured microbial community. However, it remains unclear if *Roseiflexus* CIS is targeted towards cyanobacteria in eCIS-like manner or whether it acts as a self-targeted system controlling the *Roseiflexus* population in response to niche-specific conditions.

## Acknowledgements

ScopeM is acknowledged for instrument access at ETH Zürich. Functional Genomics Center Zürich is acknowledged for mass spectrometry services and support. Authors acknowledges Dr. David Kaftan

Downloaded from https://academic.oup.com/ismej/article/20/1/wrag021/8471199 by guest on 16 March 2026

and Jason Lawrence Dean at Institute of Microbiology of the Czech Academy of Sciences for organising the first sampling campaign.

## Author contributions

VAG (Conceptualization, Data Curation, Formal Analysis, Investigation, Methodology, Project Administration, Resources, Supervision, Validation, Visualization, Writing—original draft, Writing—review & editing). CH (Data Curation, Investigation, Methodology, Resources, Validation, Visualization, Writing—original draft, Writing—review & editing). IM and CVA (Data Curation, Investigation, Methodology, Validation, Visualization, Writing—review & editing). JL (Investigation). MP (Conceptualization, Funding Acquisition, Project Administration, Resources, Supervision, Writing—review & editing). MK (Funding Acquisition, Project Administration, Resources, Writing—review & editing)

## Supplementary material

Supplementary material is available at *The ISME Journal* online.

## Conflicts of interest

The authors declare no conflicts of interest.

## Funding

MP was supported by the European Research Council (CoG 101000232) and the NOMIS Foundation. IM, CVA, and MK were supported by the OP JAK project Photomachines (reg. no. CZ.02.01.01/00/22_008/0004624) financed by the Czech Ministry of Education, Youth and Sports. CVA was funded by project № 25–17184K from Grant Agency of Czech Republic and by the European Union's Horizon Europe research and innovation programme under the Marie Skłodowska-Curie grant agreement ID № 101208627.

## Data availability

Example tomograms were uploaded to the Electron Microscopy Data Bank under accession numbers EMD-55856-EMD-55859, EMD-55861, EMD-55862, EMD-55866-EMD-55869 (*R. castenholzii*); EMD-55855 (*D. aquatilis*); EMD-55854 (*C. chliarophilus*); EMD-55835, EMD-55839, EMD-55841, EMD-55842, EMD-55846 (*Roseiflexus*-like cells with contracted CIS particles in the mat sample); EMD-55848, EMD-55853, EMD-55852, EMD-55851, EMD-55870, EMD-55871, EMD-55872, EMD-55873 (*Roseiflexus*-like cells with extended CIS particles in the mat sample).

Sequence data for all metagenomes generated in this work are deposited at EBI European Nucleotide Archive under the BioProject accession numbers PRJNA1041075 (yellow layer), PRJNA1041076 (green layer), PRJNA1041077 (red layer). The 16S rRNA gene amplicon sequencing data are deposited at EBI European Nucleotide Archive under the BioProject accession numbers PRJNA1307958.

The mass spectrometry proteomics data have been deposited to the ProteomeXchange Consortium via the PRIDE [62] partner repository with the dataset identifier PXD071052.

## References

1. Galán JE, Waksman G. Protein-injection machines in bacteria. *Cell* 2018;**172**:1306–18. https://doi.org/10.1016/j.cell.2018.01.034
2. Leiman PG, Basler M, Ramagopal UA. *et al.* Type VI secretion apparatus and phage tail-associated protein complexes share a common evolutionary origin. *Proc Natl Acad Sci USA* 2009;**106**:4154–9. https://doi.org/10.1073/pnas.0813360106
3. Taylor NMI, Prokhorov NS, Guerrero-Ferreira RC. *et al.* Structure of the T4 baseplate and its function in triggering sheath contraction. *Nature* 2016;**533**:346–52. https://doi.org/10.1038/nature17971
4. Basler M, Pilhofer M, Henderson GP. *et al.* Type VI secretion requires a dynamic contractile phage tail-like structure. *Nature* 2012;**483**:182–6. https://doi.org/10.1038/nature10846
5. Basler M, Ho BT, Mekalanos JJ. Tit-for-tat: type VI secretion system counterattack during bacterial cell-cell interactions. *Cell* 2013;**152**:884–94. https://doi.org/10.1016/j.cell.2013.01.042
6. Xu J, Ericson CF, Lien Y-W. *et al.* Identification and structure of an extracellular contractile injection system from the marine bacterium *Algoriphagus machipongonensis*. *Nat Microbiol* 2022;**7**:397–410. https://doi.org/10.1038/s41564-022-01059-2
7. Shikuma NJ, Pilhofer M, Weiss GL. *et al.* Marine tubeworm metamorphosis induced by arrays of bacterial phage tail–like structures. *Science* 2014;**343**:529–33. https://doi.org/10.1126/science.1246794
8. Hurst MRH, Beard SS, Jackson TA. *et al.* Isolation and characterization of the *Serratia entomophila* antifeeding prophage. *FEMS Microbiol Lett* 2007;**270**:42–8. https://doi.org/10.1111/j.1574-6968.2007.00645.x
9. Weiss GL, Eisenstein F, Kieninger A-K. *et al.* Structure of a thylakoid-anchored contractile injection system in multicellular cyanobacteria. *Nat Microbiol* 2022;**7**:386–96. https://doi.org/10.1038/s41564-021-01055-y
10. Casu B, Sallmen JW, Schlimpert S. *et al.* Cytoplasmic contractile injection systems mediate cell death in *Streptomyces*. *Nat Microbiol* 2023;**8**:711–26. https://doi.org/10.1038/s41564-023-01341-x
11. Nagakubo T, Nishiyama T, Yamamoto T. *et al.* Contractile injection systems facilitate sporogenic differentiation of *Streptomyces davawensis* through the action of a phage tapemeasure protein-related effector. *Nat Commun* 2024;**15**:4442. https://doi.org/10.1038/s41467-024-48834-9
12. Vladimirov M, Zhang RX, Mak S. *et al.* A contractile injection system is required for developmentally regulated cell death in *Streptomyces coelicolor*. *Nat Commun* 2023;**14**:1469. https://doi.org/10.1038/s41467-023-37087-7
13. Oikonomou CM, Jensen GJ. Electron cryotomography of bacterial secretion systems. *Microbiol Spectr* 2019;**7**:10.1128/microbiolspec.psib-0019-2018. https://doi.org/10.1128/microbiolspec.PSIB-0019-2018
14. Khanna K, Villa E. Revealing bacterial cell biology using cryo-electron tomography. *Curr Opin Struct Biol* 2022;**75**:102419. https://doi.org/10.1016/j.sbi.2022.102419
15. Chen L, Song N, Liu B. *et al.* Genome-wide identification and characterization of a superfamily of bacterial extracellular contractile injection systems. *Cell Rep* 2019;**29**:511–521.e2. https://doi.org/10.1016/j.celrep.2019.08.096
16. Sarris PF, Ladoukakis ED, Panopoulos NJ. *et al.* A phage tail-derived element with wide distribution among both prokaryotic domains: a comparative genomic and phylogenetic study. *Genome Biol Evol* 2014;**6**:1739–47. https://doi.org/10.1093/gbe/evu136
17. Geller AM, Pollin I, Zlotkin D. *et al.* The extracellular contractile injection system is enriched in environmental microbes and associates with numerous toxins. *Nat Commun* 2021;**12**:3743. https://doi.org/10.1038/s41467-021-23777-7
18. Gaisin VA, Grouzdev DS, Namsaraev ZB. *et al.* Biogeography of thermophilic phototrophic bacteria belonging to *Roseiflexus* genus. *FEMS Microbiol Ecol* 2016;**92**:fiw012. https://doi.org/10.1093/femsec/fiw012

Downloaded from https://academic.oup.com/ismej/article/20/1/wrag021/8471199 by guest on 16 March 2026

19. Martinez JN, Nishihara A, Lichtenberg M. *et al.* Vertical distribution and diversity of phototrophic bacteria within a hot spring microbial mat (Nakabusa Hot Springs, Japan). *Microbes Environ* 2019;**34**:374–87. https://doi.org/10.1264/jsme2.ME19047
20. Gaisin VA, Kalashnikov AM, Sukhacheva MV. *et al.* Filamentous anoxygenic phototrophic bacteria from cyanobacterial mats of Alla Hot Springs (Barguzin Valley, Russia). *Extremophiles* 2015;**19**:1067–76. https://doi.org/10.1007/s00792-015-0777-7
21. Thiel V, Wood JM, Olsen MT. *et al.* The dark side of the mushroom spring microbial mat: life in the shadow of chlorophototrophs. I. Microbial diversity based on 16S rRNA gene amplicons and metagenomic sequencing. *Front Microbiol* 2016;**7**:919. https://doi.org/10.3389/fmicb.2016.00919
22. Ward DM, Ferris MJ, Nold SC. *et al.* A natural view of microbial biodiversity within hot spring cyanobacterial mat communities. *Microbiol Mol Biol Rev* 1998;**62**:1353–70. https://doi.org/10.1128/mmbr.62.4.1353-1370.1998
23. Hanada S, Takaichi S, Matsuura K. *et al. Roseiflexus castenholzii* gen. Nov., sp. nov., a thermophilic, filamentous, photosynthetic bacterium that lacks chlorosomes. *Int J Syst Evol Microbiol* 2002;**52**:187–93. https://doi.org/10.1099/00207713-52-1-187
24. Herlemann DPR, Labrenz M, Jürgens K. *et al.* Transitions in bacterial communities along the 2000 km salinity gradient of the Baltic Sea. *ISME J* 2011;**5**:1571–9. https://doi.org/10.1038/ismej.2011.41
25. Martin M. Cutadapt removes adapter sequences from high-throughput sequencing reads. *EMBnetjournal* 2011;**17**:10–2. https://doi.org/10.14806/ej.17.1.200
26. Callahan BJ, McMurdie PJ, Rosen MJ. *et al.* DADA2: high-resolution sample inference from Illumina amplicon data. *Nat Methods* 2016;**13**:581–3. https://doi.org/10.1038/nmeth.3869
27. McMurdie PJ, Holmes S. Phyloseq: an R package for reproducible interactive analysis and graphics of microbiome census data. *PLoS One* 2013;**8**:e61217. https://doi.org/10.1371/journal.pone.0061217
28. Wickam H. *Ggplot2: Elegant Graphics for Data Analysis*. New York: Springer New York, 2009, 10.1007/978-0-387-98141-3.
29. Bolger AM, Lohse M, Usadel B. Trimmomatic: a flexible trimmer for Illumina sequence data. *Bioinformatics* 2014;**30**:2114–20. https://doi.org/10.1093/bioinformatics/btu170
30. Bankevich A, Nurk S, Antipov D. *et al.* SPAdes: a new genome assembly algorithm and its applications to single-cell sequencing. *J Comput Biol* 2012;**19**:455–77. https://doi.org/10.1089/cmb.2012.0021
31. Kang DD, Li F, Kirton E. *et al.* MetaBAT 2: an adaptive binning algorithm for robust and efficient genome reconstruction from metagenome assemblies. *PeerJ* 2019;**7**:e7359. https://doi.org/10.7717/peerj.7359
32. Parks DH, Imelfort M, Skennerton CT. *et al.* CheckM: assessing the quality of microbial genomes recovered from isolates, single cells, and metagenomes. *Genome Res* 2015;**25**:1043–55. https://doi.org/10.1101/gr.186072.114
33. Ramos-Barbero MD, Martin-Cuadrado A-B, Viver T. *et al.* Recovering microbial genomes from metagenomes in hypersaline environments: the good, the bad and the ugly. *Syst Appl Microbiol* 2019;**42**:30–40. https://doi.org/10.1016/j.syapm.2018.11.001
34. Aldeguer-Riquelme B, Antón J, Santos F. Distribution, abundance, and ecogenomics of the *Palauibacterales*, a new cosmopolitan thiamine-producing order within the *Gemmatimonadota* phylum. *mSystems* 2023;**8**:e00215–23. https://doi.org/10.1128/msystems.00215-23
35. Chaumeil P-A, Mussig AJ, Hugenholtz P. *et al.* GTDB-Tk: a toolkit to classify genomes with the genome taxonomy database. *Bioinformatics* 2020;**36**:1925–7. https://doi.org/10.1093/bioinformatics/btz848
36. Menzel P, Ng KL, Krogh A. Fast and sensitive taxonomic classification for metagenomics with kaiju. *Nat Commun* 2016;**7**:11257. https://doi.org/10.1038/ncomms11257
37. Jain C, Rodriguez-R LM, Phillippy AM. *et al.* High throughput ANI analysis of 90K prokaryotic genomes reveals clear species boundaries. *Nat Commun* 2018;**9**:5114. https://doi.org/10.1038/s41467-018-07641-9
38. Rodriguez-R LM, Konstantinidis KT. The Enveomics collection: a toolbox for specialized snalyses of microbial genomes and metagenomes. *PeerJ Preprints* 2016;**4**:e1900v1. https://doi.org/10.7287/peerj.preprints.1900v1
39. Seemann T. Prokka: rapid prokaryotic genome annotation. *Bioinformatics* 2014;**30**:2068–9. https://doi.org/10.1093/bioinformatics/btu153
40. Iancu CV, Tivol WF, Schooler JB. *et al.* Electron cryotomography sample preparation using the Vitrobot. *Nat Protoc* 2006;**1**:2813–9. https://doi.org/10.1038/nprot.2006.432
41. Zachs T, Schertel A, Medeiros J. *et al.* Fully automated, sequential focused ion beam milling for cryo-electron tomography. *elife* 2020;**9**:e52286. https://doi.org/10.7554/eLife.52286
42. Mastronarde DN. Automated electron microscope tomography using robust prediction of specimen movements. *J Struct Biol* 2005;**152**:36–51. https://doi.org/10.1016/j.jsb.2005.07.007
43. Schorb M, Haberbosch I, Hagen WJH. *et al.* Software tools for automated transmission electron microscopy. *Nat Methods* 2019;**16**:471–7. https://doi.org/10.1038/s41592-019-0396-9
44. Eisenstein F, Yanagisawa H, Kashihara H. *et al.* Parallel cryo electron tomography on *in situ* lamellae. *Nat Methods* 2023;**20**:131–8. https://doi.org/10.1038/s41592-022-01690-1
45. Kremer JR, Mastronarde DN, McIntosh JR. Computer visualization of three-dimensional image data using IMOD. *J Struct Biol* 1996;**116**:71–6. https://doi.org/10.1006/jsbi.1996.0013
46. Liu Y-T, Zhang H, Wang H. *et al.* Isotropic reconstruction for electron tomography with deep learning. *Nat Commun* 2022;**13**:6482. https://doi.org/10.1038/s41467-022-33957-8
47. Heebner JE, Purnell C, Hylton RK. *et al.* Deep learning-based segmentation of cryo-electron tomograms. *JoVE* 2022;**189**:e64435. https://doi.org/10.3791/64435
48. Meng EC, Goddard TD, Pettersen EF. *et al.* UCSF ChimeraX: tools for structure building and analysis. *Protein Sci* 2023;**32**:e4792. https://doi.org/10.1002/pro.4792
49. Katoh K, Rozewicki J, Yamada KD. MAFFT online service: multiple sequence alignment, interactive sequence choice and visualization. *Brief Bioinform* 2019;**20**:1160–6. https://doi.org/10.1093/bib/bbx108
50. Nguyen L-T, Schmidt HA, von Haeseler A. *et al.* IQ-TREE: a fast and effective stochastic algorithm for estimating maximum-likelihood phylogenies. *Mol Biol Evol* 2015;**32**:268–74. https://doi.org/10.1093/molbev/msu300
51. Kalyaanamoorthy S, Minh BQ, Wong TKF. *et al.* ModelFinder: fast model selection for accurate phylogenetic estimates. *Nat Methods* 2017;**14**:587–9. https://doi.org/10.1038/nmeth.4285
52. Hoang DT, Chernomor O, von Haeseler A. *et al.* UFBoot2: improving the ultrafast bootstrap approximation. *Mol Biol Evol* 2018;**35**:518–22. https://doi.org/10.1093/molbev/msx281
53. Letunic I, Bork P. Interactive tree of life (iTOL) v6: recent updates to the phylogenetic tree display and annotation tool. *Nucleic Acids Res* 2024;**52**:W78–82. https://doi.org/10.1093/nar/gkae268
54. Tomova I, Stoilova-Disheva M, Lyutskanova D. *et al.* Phylogenetic analysis of the bacterial community in a geothermal spring,


Downloaded from https://academic.oup.com/ismej/article/20/1/wrag021/8471199 by guest on 16 March 2026

Rupi Basin. *Bulgaria World J Microbiol Biotechnol* 2010;**26**:2019–28. https://doi.org/10.1007/s11274-010-0386-7

55. Strunecký O, Kopejtka K, Goecke F. *et al.* High diversity of thermophilic cyanobacteria in Rupite hot spring identified by microscopy, cultivation, single-cell PCR and amplicon sequencing. *Extremophiles* 2019;**23**:35–48. https://doi.org/10.1007/s00792-018-1058-z
56. Sitte H, Edelmann L, Neumann K. Cryofixation without pretreatment at ambient pressure. In: Steinbrecht R.A., Zierold K. (eds.), *Cryotechniques in Biological Electron Microscopy*. Berlin, Heidelberg: Springer, 1987, 87–113.
57. Nurk S, Meleshko D, Korobeynikov A. *et al.* metaSPAdes: a new versatile metagenomic assembler. *Genome Res* 2017;**27**:824–34. https://doi.org/10.1101/gr.213959.116
58. King CE, King GM. Description of *Thermogemmatispora carboxidivorans* sp. nov., a carbon-monoxide-oxidizing member of the class *Ktedonobacteria* isolated from a geothermally heated biofilm, and analysis of carbon monoxide oxidation by members of the class *Ktedonobacteria*. *Int J Syst Evol Microbiol* 2014;**64**:1244–51. https://doi.org/10.1099/ijs.0.059675-0
59. Raposo P, Viver T, Albuquerque L. *et al.* Transfer of *Meiothermus chliarophilus* (Tenreiro et al.1995) Nobre et al. 1996, *Meiothermus roseus* Ming et al. 2016, *Meiothermus terrae* Yu et al. 2014 and *Meiothermus timidus* Pires et al. 2005, to *Calidithermus* gen. Nov., as *Calidithermus chliarophilus* comb. nov., *Calidithermus roseus* comb. nov., *Calidithermus terrae* comb. nov. and *Calidithermus timidus* comb. nov., respectively, and emended description of the genus *Meiothermus*. *Int J Syst Evol Microbiol* 2019;**69**:1060–9. https://doi.org/10.1099/ijsem.0.003270
60. Tenreiro S, Nobre MF, Costa DA. *et al. Thermus silvanus* sp. nov. and *Thermus chliarophilus* sp. nov., two new species related to *Thermus ruber* but with lower growth temperatures. *Int J Syst Evol Microbiol* 1995;**45**:633–9. https://doi.org/10.1099/00207713-45-4-633
61. Casu B, Sallmen JW, Haas PE. *et al.* Function and firing of the *Streptomyces coelicolor* contractile injection system requires the membrane protein CisA. *elife* 2025;**14**:RP104064. https://doi.org/10.7554/eLife.104064
62. Perez-Riverol Y, Bandla C, Kundu DJ. *et al.* The PRIDE database at 20 years: 2025 update. *Nucleic Acids Res* 2025;**53**:D543–53. https://doi.org/10.1093/nar/gkae1011

Downloaded from https://academic.oup.com/ismej/article/20/1/wrag021/8471199 by guest on 16 March 2026

© The Author(s) 2026. Published by Oxford University Press on behalf of the International Society for Microbial Ecology. This is an Open Access article distributed under the terms of the Creative Commons Attribution License (https://creativecommons.org/licenses/by/4.0/), which permits unrestricted reuse, distribution, and reproduction in any medium, provided the original work is properly cited.
*The ISME Journal*, 2026, **20(1)**, wrag021
https://doi.org/10.1093/ismejo/wrag021
Original Article